The intelligent knife (iKnife) and its intraoperative diagnostic advantage for the treatment of cervical disease

Menelaos Tzafetas[a,b,c], Anita Mitra[a,b,c], Maria Paraskevaidi[a,b], Zsolt Bodai[a,b], Ilkka Kalliala[a,b,d], Sarah Bowden[a,b,c], Konstantinos Lathouras[c], Francesca Rosini[a,b], Marcell Szasz[e], Adele Savage[a,b], Eftychios Manoli[f], Julia Balog[a,b,g], James McKenzie[a,b], Deirdre Lyons[c], Phillip Bennett[a,b,c], David MacIntyre[a,b], Sadaf Ghaem-Maghami[a,b,c], Zoltan Takats[a,b,1,2], and Maria Kyrgiou[a,b,c,1,2]

[a]Department of Metabolism, Digestion and Reproduction, Institute of Reproductive and Developmental Biology, Faculty of Medicine, Imperial College London, London SW7 2DD, United Kingdom; [b]Department of Surgery and Cancer, Institute of Reproductive and Developmental Biology, Faculty of Medicine, Imperial College London, London SW7 2DD, United Kingdom; [c]Department of Obstetrics and Gynaecology, Imperial College Healthcare NHS Trust, London W2 1NY, United Kingdom; [d]Department of Obstetrics and Gynaecology, University Hospital Helsinki, Helsinki University, 00290 Helsinki, Finland; [e]Department of Tumour Biology, National Koranyi Institute of Pulmonology, 1122 Budapest, Hungary; [f]Department of Metabolism, Digestion and Reproduction, Imperial College London, London SW7 2DD, United Kingdom; and [g]Waters Research Center, 1031 Budapest, Hungary

Edited by Dennis A. Carson, University of California San Diego, La Jolla, CA, and approved February 14, 2020 (received for review September 29, 2019)

Clearance of surgical margins in cervical cancer prevents the need for adjuvant chemoradiation and allows fertility preservation. In this study, we determined the capacity of the rapid evaporative ionization mass spectrometry (REIMS), also known as intelligent knife (iKnife), to discriminate between healthy, preinvasive, and invasive cervical tissue. Cervical tissue samples were collected from women with healthy, human papilloma virus (HPV) ± cervical intraepithelial neoplasia (CIN), or cervical cancer. A handheld diathermy device generated surgical aerosol, which was transferred into a mass spectrometer for subsequent chemical analysis. Combination of principal component and linear discriminant analysis and least absolute shrinkage and selection operator was employed to study the spectral differences between groups. Significance of discriminatory *m/z* features was tested using univariate statistics and tandem MS performed to elucidate the structure of the significant peaks allowing separation of the two classes. We analyzed 87 samples (normal = 16, HPV ± CIN = 50, cancer = 21 patients). The iKnife discriminated with 100% accuracy normal (100%) vs. HPV ± CIN (100%) vs. cancer (100%) when compared to histology as the gold standard. When comparing normal vs. cancer samples, the accuracy was 100% with a sensitivity of 100% (95% CI 83.9 to 100) and specificity 100% (79.4 to 100). Univariate analysis revealed significant MS peaks in the cancer-to-normal separation belonging to various classes of complex lipids. The iKnife discriminates healthy from premalignant and invasive cervical lesions with high accuracy and can improve oncological outcomes and fertility preservation of women treated surgically for cervical cancer. Larger in vivo research cohorts are required to validate these findings.

REIMS | cervical cancer | mass spectrometry | iKnife | fertility preservation

Cervical cancer remains the second commonest female cancer type in developed countries despite screening programs (1, 2). It primarily affects young, sexually active women, with almost one-fourth being diagnosed under the age of 40 y (3, 4). The impact of treatment in long-term side effects, sexual function, and quality of life is of outmost importance when compared to malignancies with a later onset. With the advent of screening, the majority of cervical cancer cases in Western societies are detected by screening and often diagnosed at early stages with small-volume disease and are amenable to surgical treatment. However, the age of women with the highest rates of cervical malignancy diagnosis (25 to 29 y) (5) corresponds to that of women at their first childbirth (United Kingdom, 28.6 y) (6). Fertility-sparing options that minimize reproductive morbidity present a critical new challenge.

Survival outcomes following surgical management of presumed early-stage cervical cancer have been shown to be equivalent to those of radical chemoradiation (7, 8). The combination of both treatment strategies does not improve oncological outcomes and substantially increases postoperative morbidity (9). While careful preoperative selection of surgical candidates who are unlikely to require adjuvant radiation is clearly required, intraoperative management is also critical. If disease is present in the pelvic lymph nodes (13 to 32% of cases) (10, 11), or is involved in or close to surgical margins in the vagina or parametrium, adjuvant radiotherapy may be necessary, which carries substantial increase in morbidity, particularly bowel and bladder side effects (12). The

Significance

Clearance of surgical margins in early cervical cancer prevents the need for adjuvant chemoradiation and associated morbidity and allows fertility preservation. Clearance of disease is also crucial in the surgical management of local recurrence of cervical tumors with exenterative surgery. In this study intelligent knife technology was able to discriminate healthy from abnormal lesions on the cervix with high accuracy, highlighting the potential to improve intraoperative management of women treated surgically for cervical cancer and, as a result, patient outcomes. While pilot experiments in vivo are encouraging, accuracy remains to be validated in larger patient cohorts. Future studies could also explore whether this technology could be used for management of cervical preinvasive disease.

Author contributions: Z.T. and M.K. designed research; M.T., Z.B., I.K., S.B., K.L., A.S., E.M., J.B., and M.K. performed research; M.T., A.M., Z.B., I.K., S.B., K.L., F.R., M.S., A.S., E.M., J.B., D.L., D.M., S.G.-M., Z.T., and M.K. contributed new reagents/analytic tools; M.T., Z.B., F.R., M.S., A.S., E.M., J.B., J.M., and M.K. analyzed data; and M.T., A.M., M.P., P.B., D.M., S.G.-M., Z.T., and M.K. wrote the paper.

Competing interest statement: Waters Corporation provided supplies and maintenance for the mass spectrometry equipment used. Z.T. serves as a paid consultant for Waters Corporation. J.B. is employed by Waters Corporation.

This article is a PNAS Direct Submission.

Data deposition: The datasets for the models used in this study are available at Figshare (https://figshare.com/articles/N_vs_HPV_CIN_vs_Ca-ALL_Samples_data_csv/11367458/1).

[1]Z.T. and M.K. contributed equally to this work.

[2]To whom correspondence may be addressed. Email: m.kyrgiou@imperial.ac.uk or z.takats@imperial.ac.uk.

This article contains supporting information online at https://www.pnas.org/lookup/suppl/doi:10.1073/pnas.1916960117/-/DCSupplemental.

First published March 16, 2020.

rates of close (<5 mm) or positive surgical margins at radical hysterectomy have been reported as high as 63% (13). In fertility-sparing surgery, rates of positive margins have been reported as high as 9.8% (2.3 to 60%) (13–15). In fertility-sparing surgery, presence of disease at the endocervical margin at the level of the isthmus necessitates hysterectomy and/or radiotherapy and fertility loss and happens in 1 in 10 women (16). Clearance of disease is also crucial in the surgical management of local recurrence of cervical tumors (17).

Frozen section remains the only intraoperative diagnostic method for margin clearance and assessment of suspicious pelvic lymph nodes. The method has variable accuracy, partly due to the subjective nature of pathology-dependent assessment. Concordance with final histopathology has been reported at 84% (18). It requires organization and infrastructure to support the service and prolongs operating time.

Innovative technologies such as rapid evaporative ionization mass spectrometry (REIMS), also known as the intelligent knife (iKnife) (19), have been developed to aid tissue-type identification. REIMS is an ambient ionization MS technique developed for the chemical analysis of electrosurgery-generated aerosols. The molecular ionic species generated by REIMS are analyzed by time-of-flight (ToF) MS to provide tissue identification in nearly real time (20). The surgical aerosol is generated directly from tissue surfaces using standard electrosurgery devices without need for sample preparation, presenting potential use for intraoperative diagnosis. Dysregulation of lipid metabolism is associated with many cancers (21) and has been readily detected by REIMS in a number of tissue types (22). The iKnife technology robustly (100% accuracy) discriminates cancer from normal tissue in different tumor sites including the brain, breast, ovaries, and colon (19, 23–27).

The aim of this study was to assess whether the iKnife has the potential to enhance intraoperative management during the surgical treatment of early-stage cervical cancer by accurately discriminating between healthy, preinvasive, and invasive cervical tissue ex vivo.

Results

We collected 103 patient samples (normal = 27; human papilloma virus [HPV] ± cervical intraepithelial neoplasia [CIN] = 53; cancer = 23); 16 were excluded (Fig. 1). A total of 87 samples were included in the final analysis: normal (n = 16), HPV ± CIN (n = 50), and cancer (n = 21) (28). Patient characteristics are presented in Table 1. Dependent on the biopsy size (1 × 1 to 5 × 10 mm), we produced from one to seven analysis points per sample with a total of 209 MS spectra/points (normal = 25, HPV ± CIN = 123, cancer = 61) (Fig. 2 and *SI Appendix*, Tables S1 and S2).

Supervised linear discriminant analysis (LDA), following least absolute shrinkage and selection operator (LASSO) feature selection, results in complete separation among the three groups (Fig. 3*A*), with the resulting scores plot showing separation of malignant and normal cervical tissues along the second linear discriminant (LD2) (y axis), whereas the HPV ± CIN group was separated from normal along the first linear discriminant (LD1) (x axis) (Fig. 3*A*). An overall classification of 100% was achieved for iKnife-based identification of the three main groups (Fig. 3*B*). The model correctly classified normal, HPV ± CIN cervical tissue, and cancer in 100% of cases (Fig. 3*B*).

Subgroup analyses of individual paired comparisons allowed for calculation of diagnostic accuracy parameters for the models (Table 2). The overall accuracy of iKnife for identifying abnormal samples (including HPV, CIN, and cancer) from controls when compared to gold-standard histology was 100% (95%CI, 95.9 to 100%) with a sensitivity of 100% (94.9 to 100) and specificity of 100% (79.4 to 100) (Fig. 4 and Table 2). When we compared normal vs. cancer, the accuracy was also 100% (90.5 to 100) with sensitivity of 100%, (83.9 to 100) and specificity of 100% (79.4 to 100). The comparisons for normal vs. HPV ± CIN had an overall accuracy of 100% (94.6 to 100) with a sensitivity of 100% (92.9 to 100) and specificity of 100% (79.4 to 100). The final group compared was HPV ± CIN vs. cancer, which showed 100% (94.9 to 100) overall diagnostic accuracy, sensitivity of 100% (83.9 to 100), and specificity of 100% (92.9 to 100) (Table 2).

We further conducted univariate analysis using ANOVA and identified significant peaks in the spectral data found to show consistently increased relative intensity in cancer when compared to healthy tissue (Fig. 5). Twelve of them were further analyzed with tandem MS. The resulting fragmentation and accurate mass data were then compared to MS database data (LIPID MAPS) to tentatively identify the molecules of interest. MS peaks that contributed to the separation of malignant from normal cervical samples belong to six different lipid groups: sphingomyelins (SM) (m/z 687.533 [P = 0.0011]); phosphatidic acids (PA) (m/z 673.481 [P < 0.0001], 699.497 [P < 0.0001], and 725.512 [P < 0.0001]);

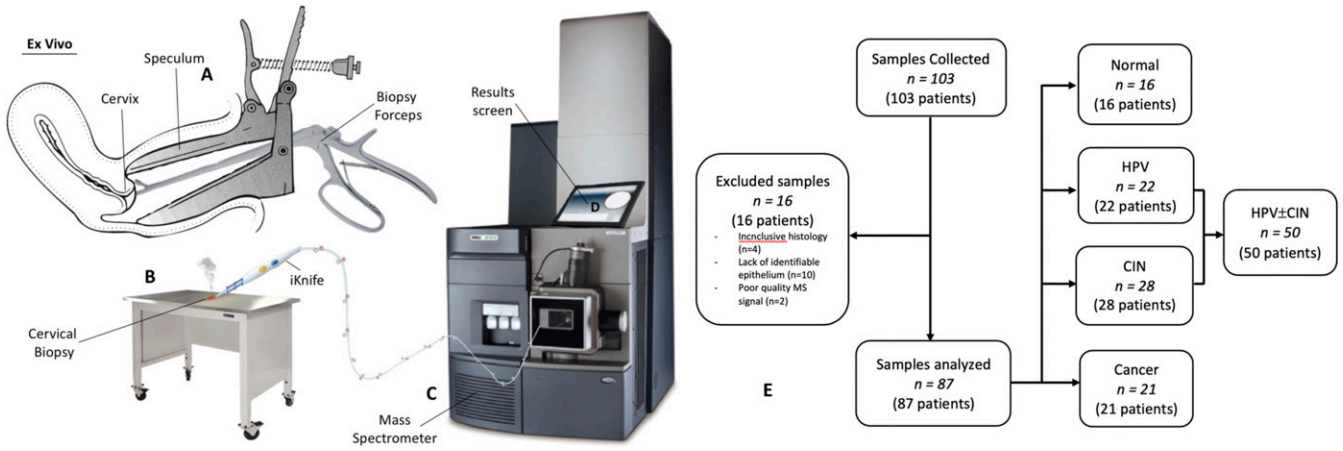

Fig. 1. Tissue collection and iKnife processing. (*A*) Cervical biopsy obtained with the use of cervical punch biopsy forceps during colposcopic assessment and snap-frozen. (*B*) Fresh frozen sample thawed to room temperature and diathermized with the iKnife, leading to ionization and aerosol (smoke) extraction of the tissue's unique lipid profile. (*C*) Aerosol produced from diathermy is transported to the mass spectrometer with the use of suction tubing. (*D*) Aerosol is processed, producing translational results on screen. (*E*) Population and samples: 103 samples from 103 patients collected; 16 samples were excluded. The analysis included 87 samples from 87 patients. HPV ± CIN included samples with HPV changes and/or CIN.

Table 1. Patient characteristics and demographics

Characteristics	Normal (n = 16)	HPV ± CIN (n = 50)	Cancer (n = 21)	Total (n = 87)
Age mean, y (range, SD)	45.3 (26–65, 10.95)	34.9 (23–58, 6.73)	50.2 (32–71, 13.47)	38.5 (23–71)
Ethnicity, *n/N* (%)				
Caucasian	13/16 (81.3)	42/50 (84.0)	19/21 (90.5)	74/87 (85.1)
Black	2/16 (12.5)	4/50 (8.0)	2/21 (9.5)	8/87 (9.2)
Asian	1/16 (6.2)	4/50 (8.0)	0/21 (0.0)	5/87 (5.7)
Parity, *n/N* (%)				
Nulliparous	9/16 (56.3)	37/50 (74.5)	5/21 (23.8)	51/87 (58.6)
Multiparous	7/16 (43.7)	13/50 (25.5)	16/21 (76.2)	36/87 (41.4)
Smoker, *n/N* (%)				
Yes	3/16 (18.6)	14/50 (27.4)	8/21 (38.1)	25/87 (28.7)
No	12/16 (75.0)	35/50 (70.6)	11/21 (52.4)	58/87 (66.7)
Ex-smoker	1/16 (6.4)	1/50 (2.0)	2/21 (9.5)	4/87 (4.6)
Menopause, *n/N* (%)				
Premenopausal	9/16 (56.3)	49/50 (98.0)	13/21 (61.9)	71/87 (81.6)
Postmenopausal	7/16 (43.7)	1/50 (2.0)	8/21 (38.1)	16/87 (18.4)
Contraception, *n/N* (%)				
Nil (sexually active)	3/16 (18.8)	13/50 (26.0)	11/21 (52.4)	27/87 (31.0)
Nil (not sexually active)	0/16 (0.0)	1/50 (2.0)	0/21 (0.0)	1/87 (1.2)
Nil (postmenopause)	6/16 (37.5)	1/50 (2.0)	6/21 (28.6)	13/87 (14.9)
Male condoms	3/16 (18.8)	15/50 (30.0)	4/21 (19.0)	22/87 (25.3)
COCP	1/16 (6.2)	12/50 (24.0)	0/21 (0.0)	13/87 (14.9)
IUS (premenopause)	2/16 (12.5)	2/50 (4.0)	0/21 (0.0)	4/87 (4.6)
IUS (postmenopause)	1/16 (6.2)	0/50 (0.0)	0/21 (0.0)	1/87 (1.2)
Implant	0/16 (0.0)	2/50 (4.0)	0/21 (0.0)	2/87 (2.3)
Progesterone-only pill	0/16 (0.0)	3/50 (6.0)	0/21 (0.0)	3/87 (3.4)
Contraceptive patch	0/16 (0.0)	1/50 (2.0)	0/21 (0.0)	1/87 (1.2)
Previous conization, *n/N* (%)				
Yes	3/16 (18.8)	2/50 (4.0)	2/21 (9.5)	7/87 (8.0)
No	13/16 (81.2)	48/50 (96.0)	19/21 (90.5)	80/87 (92.0)
HPV DNA type, *n/N* (%)				
hrHPV	4/16 (25.0)	40/50 (80.0)	6/21 (28.6)	50/87 (57.5)
lrHPV only	2/16 (12.5)	2/50 (4.0)	0/21 (0.0)	4/87 (4.6)
Negative	8/16 (50.0)	6/50 (12.0)	0/21 (0.0)	14/87 (16.1)
Unknown	2/16 (12.5)	2/50 (4.0)	15/21 (71.4)	19/87 (21.8)
Histology type, *n/N* (%)				
Normal	16/16 (100)	0/50 (0.0)	0/21 (0.0)	16/87 (18.4)
HPV	0/16 (0.0)	19/50 (38.0)	0/21 (0.0)	19/87 (21.8)
CIN1	0/16 (0.0)	4/50 (8.0)	0/21 (0.0)	4/87 (4.6)
CIN 1/2	0/16 (0.0)	4/50 (8.0)	0/21 (0.0)	4/87 (4.6)
CIN 2	0/16 (0.0)	3/50 (6.0)	0/21 (0.0)	3/87 (3.5)
CIN 2/3	0/16 (0.0)	9/50 (18.0)	0/21 (0.0)	9/87 (10.3)
CIN 3	0/16 (0.0)	11/50 (22.0)	0/21 (0.0)	11/87 (12.6)
SCC	0/16 (0.0)	0/50 (0.0)	20/21 (95.2)	20/87 (23.0)
Adenocarcinoma	0/16 (0.0)	0/50 (0.0)	1/21 (4.8)	1/87 (1.2)
Stage, *n/N* (%)				
IA1	N/A	N/A	0/21 (0.0)	0/21 (0.0)
IA2	N/A	N/A	0/21 (0.0)	0/21 (0.0)
IB1	N/A	N/A	5/21 (23.8)	5/21 (23.8)
IB2	N/A	N/A	3/21 (14.3)	3/21 (14.3)
IIA	N/A	N/A	1/21 (4.8)	1/21 (4.8)
IIB	N/A	N/A	7/21 (33.3)	7/21 (33.3)
IIIA	N/A	N/A	0/21 (0.0)	0/21 (0.0)
IIIB	N/A	N/A	2/21 (9.5)	2/21 (9.5)
IVA	N/A	N/A	3/21 (14.3)	3/21 (14.3)

Data for 16 healthy controls, 50 with HPV ± CIN, and 21 with invasive cervical cancer. COCP: combined oral contraceptive pill; hrHPV: high-risk HPV; IUS: intrauterine system; lrHPV: low-risk HPV; Nil: nothing; SCC: squamous cell carcinoma; N/A: not applicable.

phosphatidylethanolamines (PE) (m/z 744.554 [$P < 0.0001$] and 750.544 [$P = 0.0003$]); phosphatidylglycerols (PG) (m/z 747.518 [$P < 0.0001$], 771.518 [$P < 0.0001$], and 773.533 [$P < 0.0001$]); phosphatidycholine (PC) group (m/z 794.570 [$P = 0.0002$] and 818.570 [$P = 0.0004$]); and phosphatidylinositols (PI) (m/z 885.549 [$P = 0.0011$]) (Table 3).

We used the iKnife in four in vivo cases of women undergoing excisional treatment for CIN (one case of CIN1, two cases of CIN2, and one case of CIN3). Three cases had clear margins, and this was consistent with the iKnife result. The histology report suggested positive margins for CIN3 in one case of a 51-y-old woman who subsequently underwent a repeat local excisional treatment, while

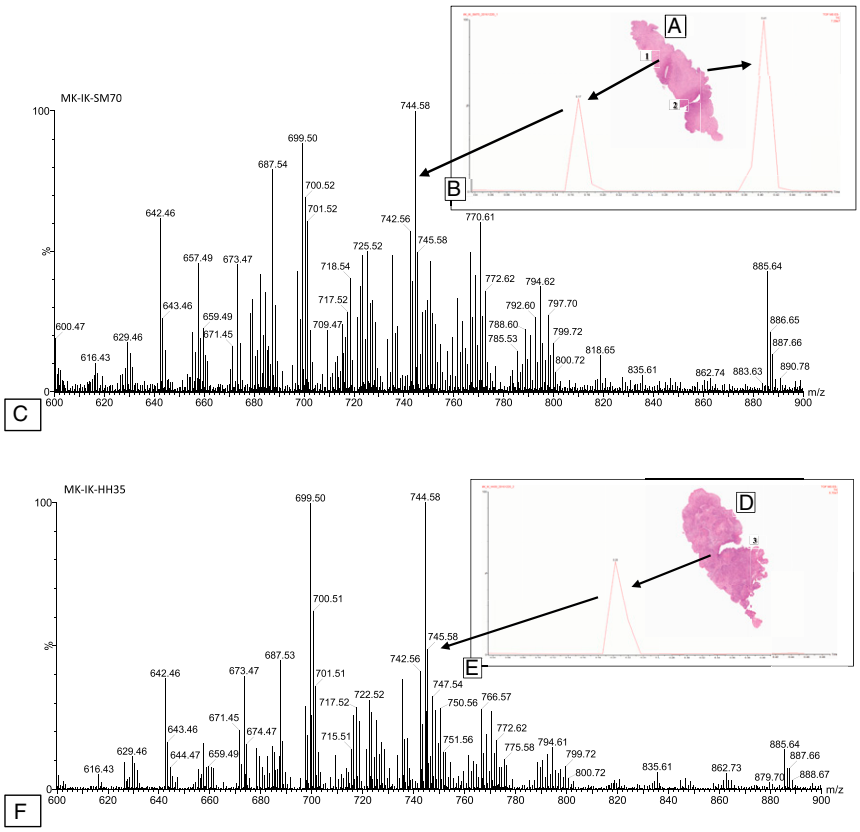

Fig. 2. iKnife analysis of benign and cancerous cervical biopsies. Benign (*A*) and malignant (*D*) uterine cervical biopsy with iKnife burns labeled (1 through 3) as the sampling sites. Total ion chromatogram (*B* = normal, *E* = cancer) obtained during the sampling of the specimen with the iKnife in the equivalent tissue type. Representative mass spectra, obtained in negative-ion mode from uterine cervical biopsies, showing the degree of variability in the peaks for different tissue types (*C* = normal, *F* = cancer). Marker explanation: Each spectral peak reflects one burn in the tissue images (1 through 3). The spectral image (*B* and *E*) is the outcome of the burn.

the iKnife reported this as clear. The repeat cone had no CIN, consistent with the iKnife result (*SI Appendix*, Fig. S1).

Discussion

In this prospective study we demonstrate that iKnife has the potential to enhance intraoperative management of women treated surgically for cervical malignancy. When compared to gold-standard histology, the iKnife achieved high sensitivity and specificity, suggesting that this could be used as an accessory diagnostic tool intraoperatively. The iKnife could differentiate HPV ± CIN and cancer from normal tissue with 100% accuracy.

Margin clearance of at least 5 mm from invasive tumor site has been associated with improved oncological outcomes in cervical cancer surgery (13, 29). When this is not achieved, adjuvant radiotherapy has been found to improve overall survival (13, 29–31) at the cost of substantial morbidity. Radiotherapy

A

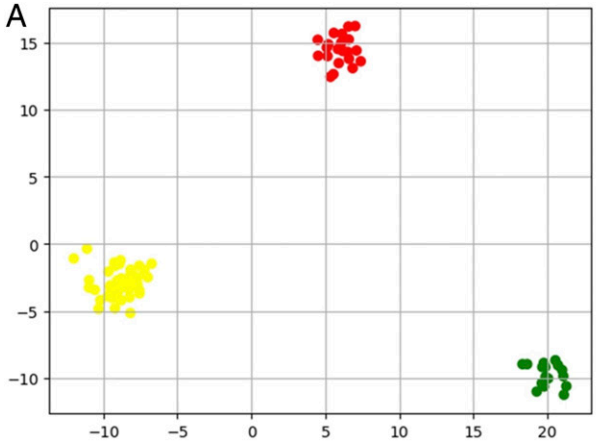

B

Proportion (%) of classification when correlating iKnife diagnosis to gold standard histology				
Predicted iKnife diagnosis	Histopathological Diagnosis			Cross Validation
	Normal (n=16)	HPV ± CIN (n=50)	Cancer (n=21)	
Normal	100% (16/16)	0% (0/50)	0% (0/21)	100%
HPV±CIN	0% (0/16)	100% (50/50)	0% (0/21)	
Cancer	0% (0/16)	0% (0/50)	100% (21/21)	

Normal Cervical Tissue
HPV ± CIN
Cancerous Cervical Tissue

Fig. 3. Multivariate analysis of obtained spectra per sample for identification of spectral differences between Normal, HPV ± CIN and Cancerous tissue. (*A*) LDA (for model normal vs. HPV ± CIN vs. cancer). (*B*) Proportion (percent) of correct classification when correlating iKnife diagnosis to gold-standard histology following LDA, leave-one-sample-out cross-validation of all samples.

Table 2. Diagnostic accuracy of REIMS iKnife for the different subgroup comparisons

	Sensitivity, % (95% CI)	Specificity, % (95% CI)	Accuracy, % (95% CI)
Normal vs. abnormal	100 (94.9–100)	100 (79.4–100)	100 (95.9–100)
Normal vs. cancer	100 (83.9–100)	100 (79.4–100)	100 (90.5–100)
Normal vs. HPV ± CIN	100 (92.9–100)	100 (79.4–100)	100 (94.6–100)
HPV ± CIN vs. cancer	100 (83.9–100)	100 (92.9–100)	100 (94.9–100)

can adversely affect quality of life and lead to vaginal stenosis, sexual dysfunction, and bowel and bladder symptoms (32, 33). Clearance of cervical preinvasive disease is also important in the context of surgery for invasive cervical cancer as positive margins may increase the risk of invasive vaginal cancer (34). Our data suggest that in vivo application of the iKnife in a surgical setting could enhance clearance of margins at excision with intraoperative nearly real-time confirmation with high accuracy. The advantages of this technique are particularly prominent in women undergoing fertility-sparing surgery where margin clearance at the uterine isthmus is required. The iKnife could also be of use in the exenterative surgery for local recurrences. Although surgery aims for complete tumor clearance (R0), positive margins are associated with significantly worse disease-free and overall survival rates (17). Exenterative surgery is highly morbid and frequently demands formation of two permanent stomas (colostomy and urostomy); surgical clearance is therefore crucial.

The iKnife may have further applications in other gynecological malignancies. Surgical excision with clear margins for vulvar cancer, for instance, can be challenging as the presence of disease cannot always be seen macroscopically, while extensive excision in the absence of disease may have substantial impact on future sexual function. Future uses may include real-time diagnosis of cervical biopsies or clearance of margins at local excision for cervical preinvasive neoplasia (CIN) in the colposcopy clinics, which would eliminate waiting for results and may facilitate use of "see-and-treat" approaches with local excision in clinically suitable cases in colposcopy (35–37).

Although not tested in this study, the iKnife approach could potentially be expanded to explore the accuracy of detection of metastases in lymph nodes thought suspicious at the time of surgery. Positive lymphadenopathy at the time of cervical cancer surgery dictates abandoning the surgical procedure to minimize morbidity from receiving both surgical and radiotherapy treatments (9, 38). However, the use of frozen section in this setting has limitations. Incorrect diagnoses have been shown to be as high as 15%, while accuracy is often operator-dependent. In this study the iKnife had accuracy that was better than that reported for frozen section when compared to gold-standard histology between malignant and healthy tissue. Frozen section requires infrastructure (39) and prolongs operating time (29, 39), while the iKnife can give nearly real-time (3 s) diagnosis without any tissue preparation, allowing immediate excision of further tissue if deemed necessary by the surgeon. A future surgical model may include sentinel lymph node dissection, which is currently tested in clinical trials (40), with on-the-spot iKnife diagnosis of presence of disease. Future research should explore the accuracy of the iKnife in detecting metastatic spread in lymph nodes that could be of value in other gynecological malignancies beyond cervical disease (endometrial, ovarian, and vulvar cancer).

In this study we aimed to explore the ability of the iKnife to discriminate normal from preinvasive and invasive cervical tissue. Most benign and CIN samples were collected in outpatient clinics, while cancers from advanced tumors were not amenable to surgery. We next tested the feasibility of in vivo application in a pilot cohort of four women with CIN undergoing excision. The iKnife was in agreement in three cases of clear margins but also documented

A

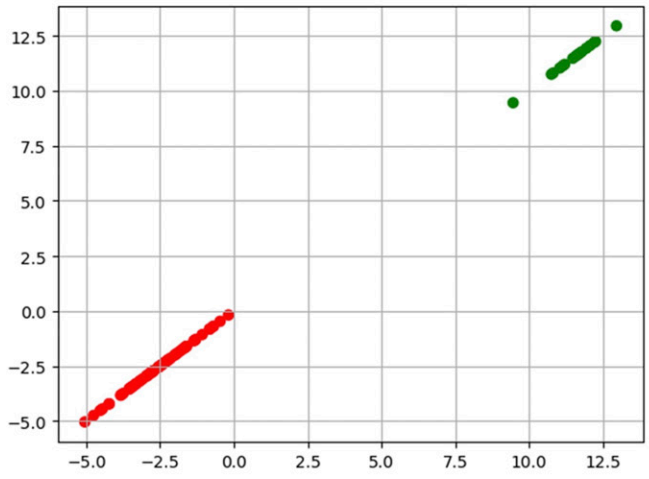

B

Proportion (%) of correct classification when correlating iKnife diagnosis to gold standard histology			
Predicted iKnife diagnosis	Histopathological Diagnosis		Cross Validation (CI%)
(a)	Normal (n=16)	Abnormal (n=71)	
Normal	100% (16)	0% (0)	100% (95.9 to 100)
Abnormal	0% (0)	100% (71)	
(b)	Normal (n=16)	Cancer (n=21)	
Normal	100% (16)	0% (0)	100% (90.5% to 100)
Cancer	0% (0)	100% (21)	
(c)	Normal (n=16)	HPV±CIN (n=50)	
Normal	100% (16)	0% (0)	100% (94.6 to 100)
HPV±CIN	0% (0)	100% (50)	
(d)	HPV±CIN (n=50)	Cancer (n=21)	
HPV±CIN	100% (50)	0% (0)	100% (94.9 to 100)
Cancer	0% (0)	100% (21)	

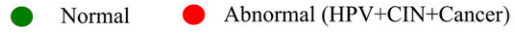

Fig. 4. (*A*) LDA multivariate analysis of obtained spectra per sample for identification of spectral differences between normal and abnormal (HPV ± CIN or cancerous) tissue. (*B*) Proportion (percent) of correct classification when correlating iKnife diagnosis to gold-standard histology following PC-LD analysis. Leave-one-sample-out cross-validation: (*a*) normal (normal cervical tissue) vs. abnormal (HPV + CIN + cancer); (*b*) normal vs. cancer; (*c*) normal vs. HPV ± CIN; (*d*) HPV ± CIN vs. cancer.

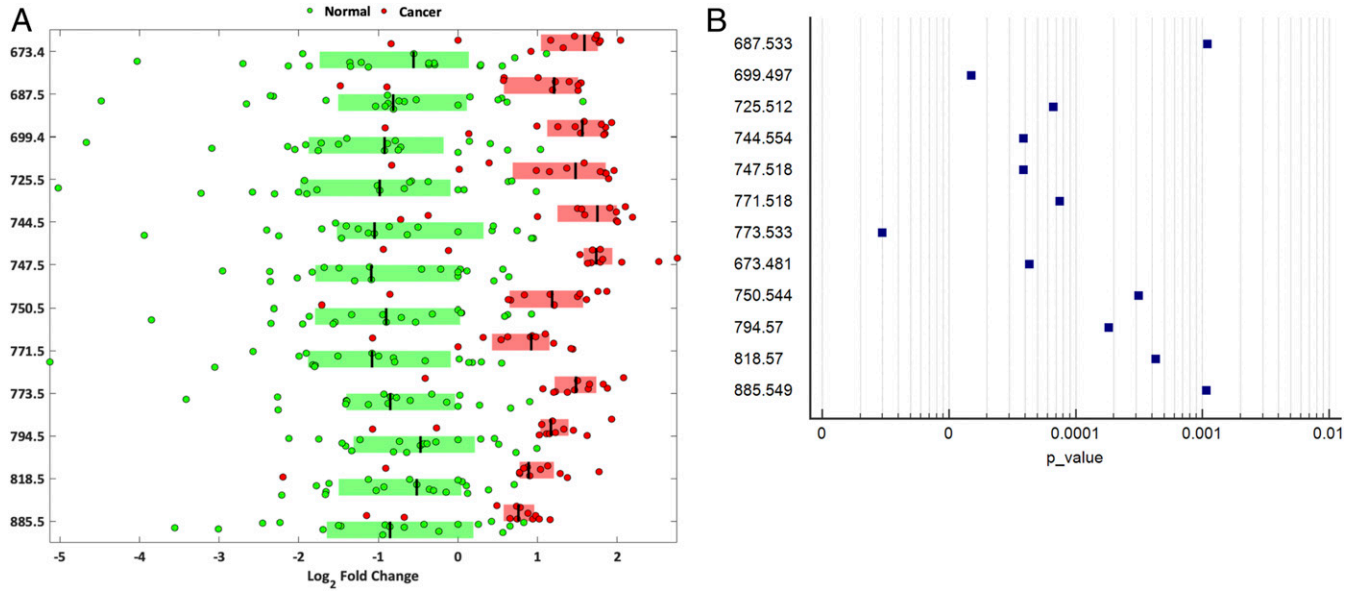

Fig. 5. Lipid groups of the identified 12 significant peaks. (*A*) Box plots of the top *m/z* peaks contributing to class separation (log_2 fold change), based on the univariate analysis between normal and cancerous cervical tissue. The log2 fold changes are determined based on the median spectrum over all observations. The 12 most significant and intense REIMS spectra peaks are shown with $P < 0.001$, $q < 0.001$. (*B*) Forest plot of the *P* values of the 12 significant peaks identified during the univariate analysis between normal and cancerous cervical tissue.

clearance of the margins in the fourth case, while the histology reported positivity for CIN3 at the endocervical margins. The woman had a repeat excision as per national recommendations (National Health Service Cervical Screening Programme guidelines) which returned a result of no residual CIN, consistent with the iKnife diagnosis (41). A possible reason for the observed discrepancy in this case could be due to the destructive nature of the diathermy, which compromises the pathologist's ability to examine the true margins of excision and positivity can therefore be overcalled, leading to unnecessary treatments (42–44). Studies have shown a much larger depth of thermal artifact after large loop excision of the transformation zone (LLETZ) beyond the excision margin, which has been reported as high as 0.85 mm (±0.94) for endocervical, 0.57 mm (±0.47) for the ectocervical, and 0.49 mm (±0.51) for the stromal margin (42). When LLETZ was compared to cold knife conization in another study, there was artifact in 61% of cases that affected at least one aspect of the excision evaluation (margin, grade, etc.) (43). In another study 10% of the ectocervical and 44% of the endocervical margin was compromised by thermal artifact (44). The iKnife offers the advantage of more accurate assessment of the true margin of the dissection. Although the results of our in vivo pilot study are encouraging, the value of the iKnife for real-time, in vivo determination of margin requires validation in a larger patient cohort.

In this study we used the LASSO model for statistical analysis. Although there are multiple ways of analyzing large datasets using machine learning tools, robust and simple methods are advised in the case of underpowered models with a small amount of data points. While principal component analysis (PCA) is an unsupervised tool to emphasize the deviation within a large dataset and is often used for dimension reduction, LASSO is a supervised and robust tool used for feature selection (and dimension reduction) of datasets containing significantly fewer data points than dimensions. In our case, there was more than an order of magnitude difference in the number of dimensions ($d = 4{,}000$) and the number of samples ($n = 87$). Although this is not ideal for most of the machine learning algorithms, LASSO has been used successfully in similar cases (i.e., ovarian cancers) (45). LASSO algorithm focuses on the features differentiating between the given classes, and thus it can be more accurate compared to PCA in cases when the model contains more classes and the deviation between the classes is not that significant. A future cross-continental multisite study will be required to cross-validate results in a large dataset to

Table 3. Tentative lipid assignments for the top 12 significant lipids in the cancer vs. normal model

m/z	*P* value	Lipid	Ion
673.481	<0.0001	Phosphatidic acid (16:0/18:1)	$[M - H]^-$
687.533	=0.0011	Sphingomyelin (d18:1/16:0)/phosphatidic acid (*O*-18:0/18:1)	$[M - CH_3]^-/[M - H]^-$
699.497	<0.0001	Phosphatidic acid (18:1/18:1)	$[M - H]^-$
725.512	<0.0001	Phosphatidic acid (18:0/20:3)/(20:2/18:1)	$[M - H]^-/[M - H]^-$
744.554	<0.0001	Phosphatidylethanolamine (18:0/18:1)/phosphatidylcholine (18:1/16:0)	$[M - H]^-/[M - CH_3]^-$
747.518	<0.0001	Phosphatidylglycerol (18:1/16:0)/phosphatidic acid (18:1/22:5)	$[M - H]^-/[M - H]^-$
750.544	=0.0003	Phosphatidylethanolamine (P-18:0/20:4)/(P-16:0/22:4)	$[M - H]^-/[M - H]^-$
771.518	<0.0001	Phosphatidylglycerol (18:2/18:1)	$[M - H]^-$
773.533	<0.0001	Phosphatidylglycerol (18:1/18:1)/(20:2/16:0)	$[M - H]^-/[M - H]^-$
794.570	=0.0002	Phosphatidylcholine (16:0/22:4)/(18:0/20:4)	$[M - CH_3]^-/ [M - CH_3]^-$
818.570	=0.0004	Phosphatidylcholine (20:2/20:4)	$[M - CH_3]^-$
885.549	=0.0011	Phosphatidylinositol (18:0/20:4)	$[M - H]^-$

explore deviation between different sites, countries, continents, and so on.

Lipid metabolism is known to be dysregulated in cancer cells, not only to support the rapid growth and division of malignant tissues but also but being involved in numerous aberrant signaling pathways required for malignant transformation, angiogenesis, and stromal invasion (46). Our study has shown that the iKnife was able to differentiate between healthy and malignant cervical tissue using signals corresponding to species, which belong to different complex lipid groups in keeping with previously published reports (21, 47, 48). Preetha et al. (21) demonstrated a significant elevation of PC, PE, PG, PI, and SM in cervical cancer vs. normal tissue using thin-layer chromatography and phosphorus assay technique. PE and SM have been found in cervical cancers with worse prognosis (49), supporting the concept that these lipid derangements play a role in the disease pathophysiology and outcomes. SM is known to regulate cell proliferation and survival through inhibition of proapoptotic pathways via the MAPK/ERK pathways, and PA similarly regulates apoptotic pathways (50). In cell culture models, the HPV-16 E7 oncoprotein has been shown to stimulate production and activation of phospholipase D, resulting in PA production, which stimulates the mTOR pathway, promoting cell proliferation (51). PA is generated through hydrolysis of PC, which has similarly been shown to be up-regulated in cervical cancer tissues (52). PI is a critical component of the PI3K/AKT/mTOR signaling pathway and aberrant signaling through this pathway is crucial for the ongoing growth and survival of numerous cancers and is a poor prognostic indicator (53).

It is currently unknown at which point lipid metabolism is significantly altered in the carcinogenesis timeline of HPV-infected cervical tissue. We hypothesize that the prevalence of phosphatidilcholine and sphingomyelin, which have been shown to have statistically significantly raised levels in the malignant cohort of our study, could indicate a metabolic pathway link to cervical carcinogenesis. Further investigation of this temporality may be useful to employ these lipids as biomarkers to predict future progressive potential, and the lipids themselves could present future therapeutic targets.

This study explored the value of innovative near-real-time spectrometry techniques in the surgical management of women with cervical neoplasms. We included a cohort with representative samples from women with cervical preinvasive and invasive disease as well as healthy controls. We further processed 12 of the significant peaks to allow for characterization of the overexpressed molecules, allowing exploration of the molecular pathways involved. We applied quality checks and excluded samples with poor-quality signal. All processed samples were reported by an expert pathologist.

There were, of course, limitations. Despite the use of an expert pathologist to validate all processed samples, the diagnosis relied on the surrounding tissue. Given the destructive nature of the technique, histological assessment from the thermally ablated tissue is not possible.

Despite encouraging findings, translation of the technique to clinical settings may be limited by current size and cost considerations, which would necessitate its use in centralized locations within hospitals and operating theaters with controlled temperature due to the limited mobility of the equipment. The current iKnife apparatus occupies a substantial footprint similar to that required for robot-assisted surgery (19, 23–26); however, future refinement of the technology toward a smaller, more user-friendly apparatus is achievable.

The results of our study suggest that innovative MS with iKnife has the potential to improve the intraoperative management of women with cervical malignancy, with intraoperative information that can minimize morbidity and enhance fertility-sparing surgical outcomes. Future larger research cohorts of in vivo samples are required to validate the technique.

Materials and Methods

Population and Samples. We included prospectively collected fresh frozen cervical tissue samples at Imperial College London (ICL) between 2016 and 2018. Samples were collected from women with normal cervix, HPV infection, CIN, and cervical cancer. The study received ethical approval from ICL Research and Ethics Committee (REC reference 13/LO/0126). The samples collected were deidentified prior to use. In cervical cancer cases, punch biopsy samples were collected at the time of staging examination under anesthesia or at the time of radical surgery. All cases were staged based on the International Federation of Gynecology and Obstetrics 2009 classification (54). For women with CIN, biopsies were taken in the colposcopy clinic, while controls were biopsied at the time of hysterectomy for benign gynecological conditions. We excluded samples that did not include epithelium, had necrotic tissue, and in cases of discrepancy between the two histopathologists. Samples that failed quality control (e.g., poor-quality signal or incorrect identification of the set lock mass in the spectra) were also excluded from further analysis. We also included a pilot population of four women attending for excisional treatment due to low- and high-grade CIN where the technology was used in vivo.

Sample iKnife Processing. Upon collection, biopsies were immediately placed into a medical-grade polypropylene cryotube (1.5 mL) and then into isopentane on dry ice for snap-freezing. Samples were stored at −80 °C within 30 min of collection. For iKnife processing, frozen samples were thawed in batches of eight samples at a time to room temperature. The samples were processed with iKnife as previously described (20, 26, 55). A Covidien ForceTriad generator at 20 W was used with a modified electrosurgical hand-piece (iKnife) to diathermize the samples in cut mode. Surgical aerosol (smoke) was obtained by ablating tissue sampling points and transported via a Venturi air pump to a XEVO G2-XS Q-ToF mass spectrometer in negative ion mode. The instrument was calibrated daily using sodium formate solution as per the manufacturer's instructions. Isopropyl alcohol (propan-2-ol) was injected as the solvent matrix at a flow rate of 0.2 mL/min. An external lock mass of leucine enkephalin (1 ng/μL) (mass in negative-ion mode 554.2615 *m/z*), as well as an internal lock mass correction of a known phospholipid (699.497 *m/z*) was used for all samples. Scan range and time was 50 to 1,200 *m/z* and 1 s, respectively. The spectral processing was performed within the 600 to 1,000 *m/z* range for all samples. In order to identify potential cross-contamination during the processing of the samples, the mass spectrometer was kept in analysis mode. Therefore, prior to the dissection of the sample if there was cross-contamination signaling would have been identified by the mass spectrometer. Such contamination issues were not detected during our processing stage. The number of individual burns per sample was determined by the size of the tissue biopsy. Larger samples produced more than one spectrum, while smaller samples produced a single spectral data file. The pilot cohort of in vivo cases was processed by the same surgeon in a single operation list with the surgeon being blinded to the real-time result of the iKnife. The aerosol produced during the excisional treatment was transferred directly into the mass spectrometer, which produced the results in real time.

Histopathological Validation. Following iKnife processing, samples were formalin-fixed and paraffin-embedded (FFPE) and stained with hematoxylin and eosin. The resulting slides were scanned with NanoZoomer 2.0HT (Hamamatsu Photonics) for digital image acquisition. The NDP.scan3.2.12 software was used for image acquisition and the NDP.view2 software was used for image viewing. The FFPE tissue samples were subsequently reviewed and reported by two senior expert histopathologists (F.R. and M.S.); the histopathological diagnosis in the area proximal to the diathermized tissue was recorded in the database. The histological diagnosis classed our samples as normal, HPV only, CIN1, CIN2, CIN3, or cancer. The excised cone from the in vivo cases was also reported by a blinded expert histopathologist and included margin status and grade of disease in the residual undiathermized cone.

Statistical Analysis, Classification Models, and Lipid Identification. Samples were grouped into three classes for the main analysis: normal, HPV ± CIN, and invasive cervical cancer tissue. Resulting spectral data were modeled using first a LASSO for feature selection followed by an LDA for classification to explore whether the iKnife could distinguish between the different tissue types. Further pairwise comparisons of profile data were performed: normal vs. abnormal (HPV + CIN + cancer); normal vs. cancer; normal vs. HPV ± CIN; and HPV ± CIN vs. cancer. Diagnostic accuracy parameters were calculated

for the resulting models and included individual paired comparisons sensitivity (S) and specificity (Sp).

The raw files produced by the mass spectrometer were analyzed with Waters Corporation's software (Abstract Model Builder [AMX] v 1.0.1581.0; not commercially available). We used this software for lock mass correction, background subtraction, and binning of data to 0.1 Da. AMX and MATLAB (R2016a; MathWorks) were used for all multivariate analysis including PCA and LDA. The three-class model (normal vs. HPV ± CIN vs. cancer) was analyzed with the free software package Anaconda Navigator with Spyder version (3.3.2) in Python (version 3.7.1). Loading plots were generated to identify spectral features responsible for discrimination of different tissue types. Leave-one-patient-out cross-validation based on an SD multiplier of 50 was performed. We performed a quality control assessment of all processed samples (i.e., signal quality, correct identification of the set lock mass in spectra, presence of histologically confirmed epithelium, and discrepancy in the final histopathological diagnosis). GraphPad (version 8) was used to analyze the patient metadata.

The statistical system R was used to undertake a univariate analysis based on the ToF scan spectra obtained during sample processing. The differences among the malignant and healthy groups were analyzed using ANOVA. The analysis identified the peaks responsible for segregation between the two groups. A P value less than 0.05 was considered statistically significant and peaks were selected for further tandem MS investigation. Lipid identification was established based on MS/MS spectra and exact mass with the use of METLIN fragmentation (https://metlin.scripps.edu/) and LIPID Metabolite and Pathways Strategy (LIPID MAPS) Lipidomic Gateway (http://www.lipidmaps.org/).

To identify discriminatory m/z features of interest, REIMS tandem MS (REIMS/MS) using the Xevo G2-XS Q-ToF instrument was performed. Mass peaks that were identified through the univariate statistical analysis and contributed strongly to class separation in PC-LDA models were selected for fragment ion scan analysis. For this, tissue samples were processed in cut mode at a power of 20 W, using compressed air as the collision gas. Tissue sampling was performed over 5 s to gain adequate volumes of aerosol for MS/MS analysis. MS/MS negative-ion-mode spectra were used to interrogate the METLIN and LIPID MAPS online databases.

Data Availability. The datasets for the models used in this study are available at Figshare (https://figshare.com/articles/N_vs_HPV_CIN_vs_Ca-ALL_Samples_data_csv/11367458/1).

Further data are available upon request.

ACKNOWLEDGMENTS. We thank all the patients from Imperial College Healthcare National Health Service Trust (ICHT) and tissue bank who provided their tissue samples for our research project, the colposcopy team at the St. Mary's site of ICHT for their cooperation during our recruitment and sample collection process, Dr. R. F. Soares and Dr. L. Doria for their assistance with the tandem MS/MS results, and Dr. H. Kudo for assisting in the production of digital images for the histology slides used to aid diagnosis. This work was funded by grants from the Medical Research Council's Imperial Confidence in Concept Scheme (PS2857 and PS2897); European Research Council Consolidator Grant MASSLIP (CoG 617896); Biomedical Research Centre Cancer Imperial College (P83204); Imperial College Healthcare Charity (RF16\10001, to M.T. and M.K.); British Society for Colposcopy and Cervical Pathology (M.K.); National Research Development and Innovation Office of Hungary (KNN121510 and NVKP_16-1-2016-0042, to M.S.), and Waters Corporation (P53626_WSSB). The views expressed are those of the authors. The funders did not influence the study design, collection, analysis and data interpretation, writing, or decision to submit the article for publication.

1. D. Cibula *et al*., The European Society of Gynaecological Oncology/European Society for Radiotherapy and Oncology/European Society of Pathology guidelines for the management of patients with cervical cancer. *Int. J. Gynecol. Cancer* **28**, 641–655 (2018).
2. M. Arbyn, P. Autier, J. Ferlay, Burden of cervical cancer in the 27 member states of the European Union: Estimates for 2004. *Ann. Oncol.* **18**, 1423–1425 (2007).
3. M. Watson *et al*., Burden of cervical cancer in the United States, 1998-2003. *Cancer* **113** (suppl. 10), 2855–2864 (2008).
4. L. Rob, P. Skapa, H. Robova, Fertility-sparing surgery in patients with cervical cancer. *Lancet Oncol.* **12**, 192–200 (2011).
5. Cancer Research UK, Cervical cancer statistics. https://www.cancerresearchuk.org/health-professional/cancer-statistics/statistics-by-cancer-type/cervical-cancer. Accessed 22 June 2019.
6. Office for National Statistics, Births by parents' characteristics in England and Wales: 2015. https://www.ons.gov.uk/peoplepopulationandcommunity/birthsdeathsandmarriages/livebirths/bulletins/birthsbyparentscharacteristicsinenglandandwales/2015. Accessed 17 June 2019.
7. F. Landoni *et al*., Randomized study between radical surgery and radiotherapy for the treatment of stage IB-IIA cervical cancer: 20-year update. *J. Gynecol. Oncol.* **28**, e34 (2017).
8. D. Cibula *et al*., The European Society of Gynaecological Oncology/European Society for Radiotherapy and Oncology/European Society of Pathology guidelines for the management of patients with cervical cancer. *Radiother. Oncol.* **127**, 404–416 (2018).
9. F. Landoni *et al*., Randomised study of radical surgery versus radiotherapy for stage Ib-IIa cervical cancer. *Lancet* **350**, 535–540 (1997).
10. P. T. Ramirez *et al*., Minimally invasive versus abdominal radical hysterectomy for cervical cancer. *N. Engl. J. Med.* **379**, 1895–1904 (2018).
11. J. Slama, P. Dundr, L. Dusek, D. Cibula, High false negative rate of frozen section examination of sentinel lymph nodes in patients with cervical cancer. *Gynecol. Oncol.* **129**, 384–388 (2013).
12. Scottish Intercollegiate Guidelines Network, "Management of cervical cancer: A national clinical guideline" (Scottish Intercollegiate Guidelines Network, Edinburgh, UK, 2008).
13. G. A. McCann *et al*., The impact of close surgical margins after radical hysterectomy for early-stage cervical cancer. *Gynecol. Oncol.* **128**, 44–48 (2013).
14. D. Y. Cao *et al*.; China Gynecologic Oncology Group, Comparisons of vaginal and abdominal radical trachelectomy for early-stage cervical cancer: Preliminary results of a multi-center research in China. *Br. J. Cancer* **109**, 2778–2782 (2013).
15. J. B. Schlaerth, N. M. Spirtos, A. C. Schlaerth, Radical trachelectomy and pelvic lymphadenectomy with uterine preservation in the treatment of cervical cancer. *Am. J. Obstet. Gynecol.* **188**, 29–34 (2003).
16. European Society of Gynaecological Oncology (ESGO), Cervical cancer guidelines. https://www.esgo.org/media/2015/12/Cervix-GL-2017-Amended-brochure.pdf. Accessed 22 June 2019.
17. A. M. Schmidt, P. Imesch, D. Fink, H. Egger, Indications and long-term clinical outcomes in 282 patients with pelvic exenteration for advanced or recurrent cervical cancer. *Gynecol. Oncol.* **125**, 604–609 (2012).
18. K. J. Park, R. A. Soslow, Y. Sonoda, R. R. Barakat, N. R. Abu-Rustum, Frozen-section evaluation of cervical adenocarcinoma at time of radical trachelectomy: Pathologic pitfalls and the application of an objective scoring system. *Gynecol. Oncol.* **110**, 316–323 (2008).
19. J. Balog *et al*., Identification of biological tissues by rapid evaporative ionization mass spectrometry. *Anal. Chem.* **82**, 7343–7350 (2010).
20. J. Balog *et al*., Intraoperative tissue identification using rapid evaporative ionization mass spectrometry. *Sci. Transl. Med.* **5**, 194ra93 (2013).
21. A. Preetha, R. Banerjee, N. Huilgol, Surface activity, lipid profiles and their implications in cervical cancer. *J. Cancer Res. Ther.* **1**, 180–186 (2005).
22. N. Strittmatter *et al*., Characterization and identification of clinically relevant microorganisms using rapid evaporative ionization mass spectrometry. *Anal. Chem.* **86**, 6555–6562 (2014).
23. J. Alexander *et al*., A novel methodology for in vivo endoscopic phenotyping of colorectal cancer based on real-time analysis of the mucosal lipidome: A prospective observational study of the iKnife. *Surg. Endosc.* **31**, 1361–1370 (2017).
24. D. L. Phelps *et al*., The surgical intelligent knife distinguishes normal, borderline and malignant gynaecological tissues using rapid evaporative ionisation mass spectrometry (REIMS). *Br. J. Cancer* **118**, 1349–1358 (2018).
25. K. C. Sächfer *et al*., In situ, real-time identification of biological tissues by ultraviolet and infrared laser desorption ionization mass spectrometry. *Anal. Chem.* **83**, 1632–1640 (2011).
26. E. R. St John *et al*., Rapid evaporative ionisation mass spectrometry of electrosurgical vapours for the identification of breast pathology: Towards an intelligent knife for breast cancer surgery. *Breast Cancer Res.* **19**, 59 (2017).
27. K. C. Schäfer *et al*., Real time analysis of brain tissue by direct combination of ultrasonic surgical aspiration and sonic spray mass spectrometry. *Anal. Chem.* **83**, 7729–7735 (2011).
28. M. Tzafetas, Data from "REIMS cervical tissue dataset." Figshare. https://figshare.com/articles/N_vs_HPV_CIN_vs_Ca-ALL_Samples_data_csv/11367458/1. Accessed 13 December 2019.
29. N. Khanna, L. A. Rauh, M. P. Lachiewicz, I. R. Horowitz, Margins for cervical and vulvar cancer. *J. Surg. Oncol.* **113**, 304–309 (2016).
30. W. A. Peters, 3rd *et al*., Concurrent chemotherapy and pelvic radiation therapy compared with pelvic radiation therapy alone as adjuvant therapy after radical surgery in high-risk early-stage cancer of the cervix. *J. Clin. Oncol.* **18**, 1606–1613 (2000).
31. L. Rogers, S. S. Siu, D. Luesley, A. Bryant, H. O. Dickinson, Radiotherapy and chemoradiation after surgery for early cervical cancer. *Cochrane Database Syst. Rev.* **5**, CD007583 (2012).
32. L. D. Flay, J. H. Matthews, The effects of radiotherapy and surgery on the sexual function of women treated for cervical cancer. *Int. J. Radiat. Oncol. Biol. Phys.* **31**, 399–404 (1995).
33. A. Hofsjö, K. Bergmark, B. Blomgren, H. Jahren, N. Bohm-Starke, Radiotherapy for cervical cancer–Impact on the vaginal epithelium and sexual function. *Acta Oncol.* **57**, 338–345 (2018).
34. B. Strander, J. Hällgren, P. Sparén, Effect of ageing on cervical or vaginal cancer in Swedish women previously treated for cervical intraepithelial neoplasia grade 3: Population based cohort study of long term incidence and mortality. *BMJ* **348**, f7361 (2014).
35. R. M. Ebisch *et al*., Evidence supporting see-and-treat management of cervical intraepithelial neoplasia: A systematic review and meta-analysis. *BJOG* **123**, 59–66 (2016).

36. S. Tahseen, P. C. Reid, Psychological distress associated with colposcopy: Patients' perception. *Eur. J. Obstet. Gynecol. Reprod. Biol.* **139**, 90–94 (2008).
37. M. Arbyn *et al*., Incomplete excision of cervical precancer as a predictor of treatment failure: A systematic review and meta-analysis. *Lancet Oncol.* **18**, 1665–1679 (2017).
38. A. Martínez *et al*., Accuracy of intraoperative pathological examination of SLN in cervical cancer. *Gynecol. Oncol.* **130**, 525–529 (2013).
39. K. Gubbala *et al*., Results from survey to assess current trends in surgical practice in the management of women with early stage cervical cancer within the BGCS community with an emphasis on routine frozen section examination. *Int. J. Surg. Oncol.* **2017**, 2962450 (2017).
40. Canadian Cancer Trials Group, A randomized phase III trial comparing radical hysterectomy and pelvic node dissection vs simple hysterectomy and pelvic node dissection in patients with low-risk early stage cervical cancer (SHAPE). https://clinicaltrials.gov/ct2/show/NCT01658930. Accessed 15 June 2019.
41. Public Health England, "NHS cervical screening programme: Colposcopy and program management" (NHSCSP Publication No. 20, Public Health England, London, 2016).
42. S. Boonlikit, M. Yanaranop, Thermal artifact after three techniques of loop excision of the transformation zone: A comparative study. *Gynecol. Obstet. Invest.* **73**, 230–235 (2012).
43. O. B. Ioffe, S. E. Brooks, R. B. De Rezende, S. G. Silverberg, Artifact in cervical LLETZ specimens: Correlation with follow-up. *Int. J. Gynecol. Pathol.* **18**, 115–121 (1999).
44. F. J. Montz, C. H. Holschneider, L. D. Thompson, Large-loop excision of the transformation zone: Effect on the pathologic interpretation of resection margins. *Obstet. Gynecol.* **81**, 976–982 (1993).
45. M. Sans *et al*., Performance of the MasSpec Pen for rapid diagnosis of ovarian cancer. *Clin. Chem.* **65**, 674–683 (2019).
46. F. Baenke, B. Peck, H. Miess, A. Schulze, Hooked on fat: The role of lipid synthesis in cancer metabolism and tumour development. *Dis. Model. Mech.* **6**, 1353–1363 (2013).
47. A. Q. Lisboa, M. Rezende, M. I. Muniz-Junqueira, M. K. Ito, Altered plasma phospholipid fatty acids and nutritional status in patients with uterine cervical cancer. *Clin. Nutr.* **27**, 371–377 (2008).
48. L. D. Bergelson, Tumor lipids. *Prog. Chem. Fats Other Lipids* **13**, 1–59 (1972).
49. C.-Y. Hung, Glycerophospholipids and sphingolipids correlate with poor prognostic genotypes of human papillomavirus in cervical cancer: Global lipidomics analysis. *Anal. Methods* **10**, 4970–4977 (2018).
50. O. Cuvillier *et al*., Suppression of ceramide-mediated programmed cell death by sphingosine-1-phosphate. *Nature* **381**, 800–803 (1996).
51. T. Rabachini *et al*., HPV-16 E7 expression up-regulates phospholipase D activity and promotes rapamycin resistance in a pRB-dependent manner. *BMC Cancer* **18**, 485 (2018).
52. M. Z. Yin *et al*., Identification of phosphatidylcholine and lysophosphatidylcholine as novel biomarkers for cervical cancers in a prospective cohort study. *Tumour Biol.* **37**, 5485–5492 (2016).
53. A. Bahrami *et al*., The potential value of the PI3K/Akt/mTOR signaling pathway for assessing prognosis in cervical cancer and as a target for therapy. *J. Cell. Biochem.* **118**, 4163–4169 (2017).
54. S. Pecorelli, Revised FIGO staging for carcinoma of the vulva, cervix, and endometrium. *Int. J. Gynaecol. Obstet.* **105**, 103–104 (2009).
55. K. C. Schäfer *et al*., In vivo, in situ tissue analysis using rapid evaporative ionization mass spectrometry. *Angew. Chem. Int. Ed. Engl.* **48**, 8240–8242 (2009).